The transcriptional landscape of cortical interneurons underlies *in-vivo* brain function and schizophrenia risk

Kevin M Anderson[1], Meghan A Collins[1], Rowena Chin[1], Tian Ge[2,3], Monica D Rosenberg[1], Avram J Holmes[1,3,4*]

[1]Department of Psychology, Yale University, New Haven, Connecticut 06520
[2]Psychiatric and Neurodevelopmental Genetics Unit, Center for Genomic Medicine, Massachusetts General Hospital, Boston, MA 02114, USA
[3]Department of Psychiatry, Massachusetts General Hospital, Harvard Medical School, Boston, MA 02114, USA
[4]Department of Psychiatry, Yale University, New Haven, Connecticut 06520, USA
*Corresponding author.

Author contributions. KMA and AJH designed the research. KMA conducted the research. MAC, RC, MDR, TG provided analytic support. KMA and AJH wrote the manuscript and made figures. All authors edited the manuscript.

Acknowledgements: This work was supported by the National Institute of Mental Health (Grant K01MH099232 to A.J.H.), the National Science Foundation (DGE-1122492 to K.M.A.), and the National Institute on Aging (K99AG054573 to T.G.). Analyses were made possible by the high-performance computing facilities provided through the Yale Center for Research Computing. We thank B.J. Casey, Danielle Gerhard, Lauren Patrick, and Erica Ho for their feedback on early versions of the project. This work used data from the Allen Institute for Brain Science, NIH Blueprint Non-Human Primate Atlas, CommonMind Consortium, Brainspan Atlas of the Developing Human Brain, and has been conducted using the UK Biobank Resource under Application Number 25163. The Genotype-Tissue Expression (GTEx) Project was supported by the Common Fund of the Office of the Director of the National Institutes of Health, and by NCI, NHGRI, NHLBI, NIDA, NIMH, and NINDS. The data used for the analyses described in this manuscript were obtained from the GTEx Portal on 01/16/2018.

Correspondence: Avram J. Holmes, Yale University, Department of Psychology, 402 Sheffield Sterling Strathcona Hall, 1 Prospect Street, New Haven, CT 06511, Phone: 203-436-9240, Email: avram.holmes@yale.edu.

Classification: Biological Sciences: Neuroscience

Keywords: fMRI, interneuron, genetics, somatostatin, parvalbumin, schizophrenia

Abstract

Inhibitory interneurons orchestrate information flow across cortex and are implicated in psychiatric illness. Although classes of interneurons have unique functional properties and spatial distributions throughout the brain, the relative influence of interneuron subtypes on brain function, cortical specialization, and illness risk remains elusive. Here, we demonstrate stereotyped organizational properties of somatostatin and parvalbumin related transcripts within human and non-human primates. Interneuron spatial distributions recapitulate cortico-striato-thalamic functional networks and track regional differences in functional MRI signal amplitude. In the general population (n=9,627), parvalbumin-linked genes account for an enriched proportion of genome-wide heritable variance in *in-vivo* functional MRI signal amplitude. This relationship is spatially dependent, following the topographic organization of parvalbumin expression in independent post-mortem brain tissue. Finally, genetic risk for schizophrenia is enriched among interneuron-linked genes and predictive of cortical signal amplitude in parvalbumin-biased regions. These data indicate that the molecular genetic basis of resting-state brain function across cortex is shaped by the spatial distribution of interneuron-related transcripts and underlies individual differences in risk for schizophrenia.

Key Findings

1. Spatial distributions of somatostatin (*SST*) and parvalbumin (*PVALB*) are negatively correlated in mature human and non-human primate cortex, paralleling patterns observed *in utero*.
2. *SST* and *PVALB* are differentially expressed within distinct limbic and somato/motor cortico-striato-thalamic networks, respectively.
3. *In-vivo* resting-state signal amplitude is heritable in the general population and tracks relative *SST/PVALB* expression across cortex.
4. Single-nucleotide polymorphisms tied to *PVALB*-related genes account for an enriched proportion of the heritable variance in resting-state signal amplitude.
5. *PVALB*-mediated heritability of resting-state signal amplitude in the general population is spatially heterogeneous, mirroring the cortical expression of *PVALB* in independent post-mortem brain tissue.
6. Polygenic risk for schizophrenia is enriched among interneuron-linked genes and predicts resting-state signal amplitude in a manner that also follows the cortical expression of *PVALB*.

Introduction

Ramón y Cajal theorized that the functional diversity of the human brain arises, in part, from the vast assortment of neurons that pattern cortex[1]. Inhibitory interneurons are the most varied neuronal class[2], exhibiting divergent morphological and physiological properties and coordinating information flow across the brain's collective set of functional connections (functional connectome)[3,4]. Foundational cross-species animal and human work provides converging evidence for the role of interneurons in healthy brain functions as well as their dysregulation in psychiatric illnesses, including schizophrenia[5,6] and major depressive disorder[7]. The development of densely sampled gene transcriptional atlases now enables the study of cellular and molecular correlates of functional brain network architecture[8-11]. Despite these methodological advances and a clear role for interneurons in the modulation of excitatory neuron activity, relatively little is known about how the spatial distribution of interneuron subtypes shape human brain activity and associated risk for psychiatric illness.

The topographic distribution of interneuron subtypes is theorized to contribute to regional and functional network specialization, partly by altering the relative excitatory/inhibitory balance within a given patch of cortex[9,12,13]. Interneurons comprise approximately 20-30% of cortical neurons[14] and form stereotyped microcircuits with excitatory projection neurons[15]. While the precise number of interneuron subtypes is under debate, the vast majority express one of a limited set of genetic markers: somatostatin (*SST*), parvalbumin (*PVALB*), and vasoactive-intestinal peptide (*VIP;* a subset of *HTR3A* interneurons)[2]. Each molecular subtype possesses unique synaptic and functional characteristics, leading to the hypothesis that the ratio of specific interneuron classes may drive local differences in neural activity. For example, *SST* expressing interneurons preferentially target dendrites of cortical projection neurons to regulate input whereas *PVALB* expressing interneurons primarily synapse on perisomatic regions to regulate output[2,16]. Consequently, the increased presence of SST, relative to other classes of interneurons, may facilitate filtering of noisy or task-irrelevant cortical signals as well as increase recurrent excitation required for higher-order cognition[20]. Conversely, relative increases in PVALB may produce stronger feedback inhibition on excitatory neurons[13], leading to shorter activation timescales[17] suited for processing constantly changing sensorimotor stimuli. These collective results suggest that the spatial distribution of interneuron subtypes could underlie regional differences in temporal signaling across cortex, as indexed by blood oxygenation level-dependent (BOLD) functional magnetic resonance imaging (fMRI).

Establishing the organizational principles by which cellular diversity influences brain function is a long-standing challenge in neuroscience, and could provide a route to understand individual variability in the diverse processing capabilities of the human brain across health and disease. Consistent with this aim, recent translational work suggests a core role of PVALB interneurons in the biological basis of fMRI measures of *in-vivo* brain function[18]. PVALB interneurons are known to orchestrate gamma-band oscillations (30-80 Hz[19,20]), a frequency range that is tightly coupled to spontaneous BOLD fluctuations[21-25]. Optogenetic stimulation of PVALB interneurons in rodents drives rhythms in the gamma range,

impacting information processing through the synchronization of excitatory neurons[20]. In psychiatric illness, several lines of evidence suggest that decreased PVALB-mediated inhibition may serve as a core locus of disruption in schizophrenia, giving rise to the altered gamma-band signal and working memory deficits observed in the disorder[26]. However, a direct link between PVALB-related genetic variation and *in-vivo* brain activity has yet to be established. Linking cortical interneurons to individual differences in human brain function would yield deep insight into the biological basis of the hemodynamic BOLD signal, providing an engine for the discovery of functional connectome-linked genes and associated risk for illness onset.

Here, we bridge genetic, transcriptional, and neuroimaging data to advance three related lines of inquiry linking interneurons to human brain function. First, we describe the principal organizational features of *SST* and *PVALB* expression in both human and non-human primates, demonstrating a robust pattern of anti-correlation across cortex. Supporting the hypothesis that interneuron ratios contribute to functional specialization, *SST* and *PVALB* were differentially expressed within distinct limbic and somato/motor cortico-striato-thalamic functional loops, respectively. Second, we establish that the relative density of *SST* and *PVALB* tracks regional differences in brain activity across cortex. In a population-based sample of 9,627 individuals[27], genetic variation among *PVALB*-correlated genes accounted for an enriched proportion of heritable variance in resting-state signal amplitude in a manner that mirrors the spatial expression of *PVALB* in an independent analysis of post-mortem brain tissue. Critically, these discoveries suggest that the molecular genetic basis of cortical function is not spatially uniform and that genes linked to PVALB interneurons underlie heritable aspects of the BOLD response. Third, we find evidence supporting the link between PVALB interneurons and psychotic illness, demonstrating that genetic risk for schizophrenia is enriched among interneuron-linked genes while also predicting reduced resting-state signal amplitude in a spatially heterogenous manner that follows the cortical expression of *PVALB.* These data help to address a long-standing challenge of neuroscience to understand how cytoarchitecture shapes human brain function and related vulnerability for psychiatric illness.

Results

Stereotyped anti-correlation of SST and PVALB interneuron markers across cortex

The unique properties of interneuron subtypes emerge early in development and are determined, in part, by their spatial location of origin in the embryonic ganglionic eminence[28,29]. *VIP* interneurons are born within the caudal ganglionic eminence (CGE), whereas *SST* and *PVALB* interneurons originate in the medial ganglionic eminence (MGE) along negatively correlated spatial gradients[30]. Parvalbumin- and somatostatin-destined neurons differentially cluster within the dorsal and ventral MGE, respectively[31,32]. Evidence in humans[9,12] and rodents[13] indicates that *SST* and *PVALB* maintain a negative spatial correlation in adulthood, suggesting that embryonic gradients may constitute a "proto-map" of mature cortex. Although the functional consequences of a negative spatial *SST/PVALB* relationship are not well understood, the presence of replicable and evolutionarily conserved expression patterns may suggest the importance of such interneuron gradients.

To characterize interneuron topography across human and non-human primate cortex, we analyze gene expression data from the Allen Human Brain Atlas (AHBA)[33] and NIH Blueprint Non-Human Primate (NHP) Atlas [34]. Cortical tissue AHBA samples from the left (n=1,273) and right (n=428) hemispheres were analyzed. Microarrays do not give absolute estimates of gene transcription, but can measure within-probe differences across samples. *SST* and *PVALB* expression values were mean and variance normalized across cortical samples, and subtracted (i.e. *SST-PVALB*) to reveal relative expression differences (Figure 1a). Extending prior evidence of negative spatial expression relationships between *SST* and *PVALB*[9,12], these two transcripts were inversely correlated across available AHBA cortical samples (Figure 1e; r(1,699)=-0.43, p<2.2e-16). *SST* and *PVALB* distributions were organized along an anterior to posterior gradient, with relative *SST* expression greatest in orbitofrontal and medial prefrontal cortex, anterior insula, anterior cingulate, and the temporal lobe (Figure 1a-c; Supplemental Figure 1). In contrast, relative *PVALB* expression was greatest within unimodal sensory, motor, and visual cortices, as well as the parietal lobe. Histologically defined anatomical categories were used to characterize regional differences of interneuron density (Figure 1c). Median relative expression of *SST* and *PVALB* was negatively correlated across cortical subregions (r(39)=-0.87, p=1.0e-13).

Suggesting that interneuron spatial gradients are a core organizational feature of primate cortex, the negative spatial relationship between *SST* and *PVALB* was evolutionarily conserved in non-human macaque primates across individual samples (r(34)=-0.74, p≤0.001). Given that *SST* and *PVALB* interneurons originate along a stereotyped, negatively correlated spatial gradient in embryonic ganglionic eminences[32], we analyzed RNAseq data from the Brainspan Atlas of the Developing Human Brain to test whether *SST*/*PVALB* negative gradients emerge during developmental periods coinciding with major waves of interneuron colonization, approximately 10-25 post conception weeks(pcw)[35,36]. The negative correlation between *SST* and *PVALB* was absent in early-fetal (8-12 pcw; β=0.32, p=0.04) and early-midfetal (13-21 pcw; β=0.02, p=0.85) ages. Consistent with the hypothesis that mature interneuron distributions result from developmentally programmed migration patterns, we observed significant

166 negative correlations between *SST*/*PVALB* across late-fetal (24-37 pcw; β=-0.47, p=0.012), early-infancy
167 (4 months; β=-0.60, p=0.0033), mid-late childhood (8-11yrs; β=-0.52, p=0.0038), and adult (18-40yrs; β=-
168 0.35, p=0.0014) age, although not in late infancy (10 months; *b*=-0.37, p=0.36), early-childhood (1-4yrs;
169 *b*=-0.11, p=0.48), or adolescence (13-15yrs; *b*=-0.54, p=0.057). These data provide developmental
170 context as well as an external replication of the *SST/PVALB* cortical expression pattern observed in the
171 AHBA (adult human) and NHP Atlas (adult macaque) samples.

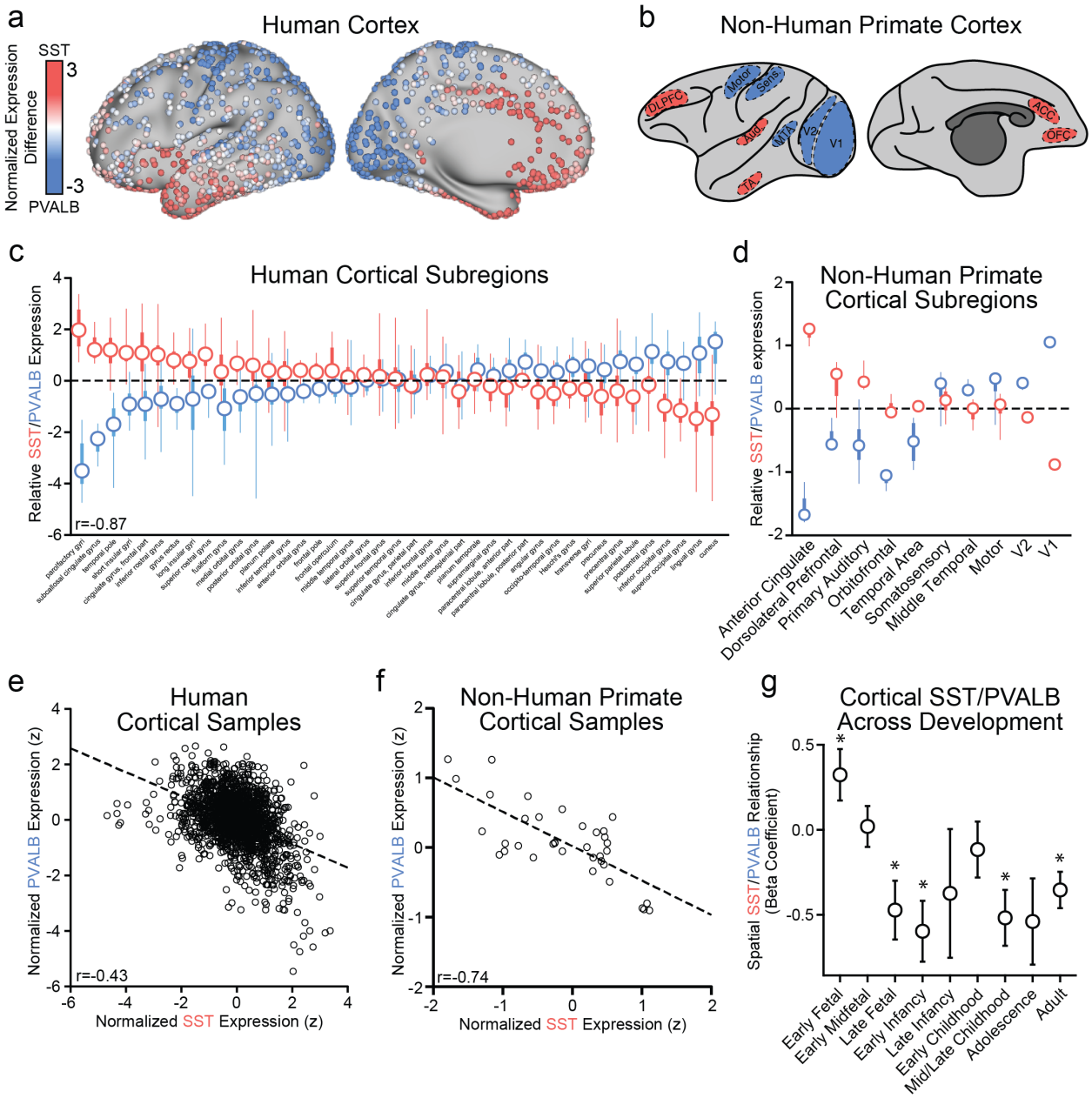

Fig 1. Cortical expression of *SST* and *PVALB* are negatively correlated across species and developmental stages. (a) Left-hemisphere AHBA tissue samples mapped to the human cortical surface, and (b) an illustration of non-human primate tissue sample locations, colored by relative expression of *SST* (red) and *PVALB* (blue). Normalized expression difference reflects the sample-wise subtraction of mean-normalized *PVALB* from *SST*. Relative *SST-PVALB* expression among anatomically defined groups from the (c) AHBA and (d) NIH Blueprint Non-Human Primate Atlas; circles=median, thick lines=interquartile range, thin lines=min and max values. (e) Sample-wise negative correlation of *SST* and *PVALB* in (e) human cortex (r=-0.43, p≤0.001) and (f) non-human primates (r=-0.74, p≤0.001). (g) Correlation of cortical *SST* and *PVALB* across nine developmental stages using data from the Brainspan Atlas of the Developing Human Brain. *p≤0.05, uncorrected; error bars=SE.

SST and _PVALB_ distinguish limbic and somato/motor cortico-striato-thalamic networks

Spatial patterns of gene expression may recapitulate the architecture of functional networks across cortex[8,10,37] and mirror functional connectivity between territories with vastly different global expression profiles (e.g., cortex and striatum[9]). We next examined whether the inverse spatial relationship between *SST* and *PVALB* is unique to cortex or preserved across subcortex (See Supplemental Information for subcortical sample information). Sample-wise expression was normalized separately for each of seven areas: striatum, thalamus, hypothalamus, globus pallidus, amygdala, hippocampus proper (i.e. CA1-CA4), and combined substantia nigra/ventral tegmentum. A cumulative negative relationship was observed between *SST* and *PVALB* (Figure 2a; r=-0.14), although a wide range of correlation values were observed (from -0.71 through 0.29). To demonstrate that the observed overall negative correlation between *SST* and *PVALB* is not obligated by global transcriptional properties, we display the distribution of averaged correlations, collapsed across cortex and the seven subcortical areas, of every gene to *SST* and to *PVALB*. Figure 2b demonstrates that *SST* is among the most negatively correlated genes to *PVALB* (bottom 0.014% of distribution), across all regions. Similarly, *PVALB* is among the most negatively correlated genes to *SST* (bottom 0.0012% of distribution). See Supplemental Figure 2 for *SST* and *PVALB* expression across subcortical subregions.

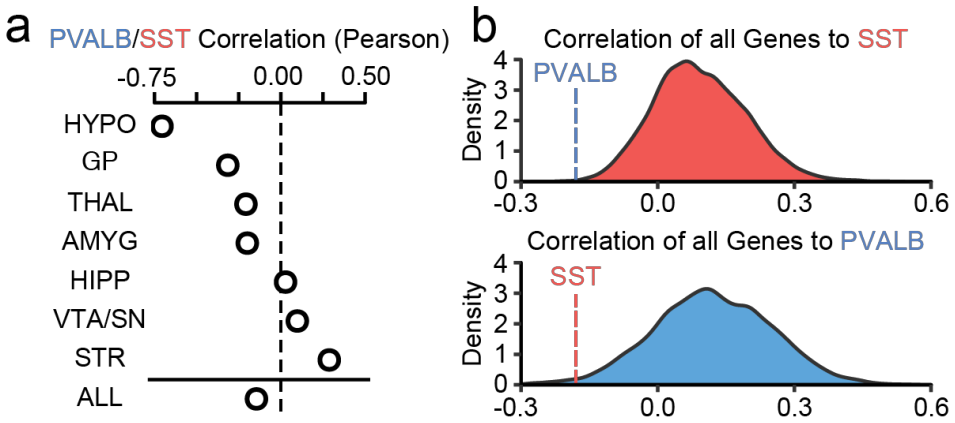

Figure 2. SST and PVALB are among the most negatively correlated transcripts to one another. (a) Overall, *SST* and *PVALB* are negatively correlated in subcortical regions (r=-0.14), but this relationship is variable (range -0.71–0.29). (b) The spatial correlation between *SST* and *PVALB* was averaged across cortex and the seven analyzed subcortical regions. Compared to all genes, *SST* and *PVALB* are among the most negatively correlated genes to one another. *PVALB* is among the top 0.0012% most negatively correlated genes to *SST* (top panel), and *SST* is among the top 0.014% most negatively correlated genes to PVALB (bottom panel). HYPO=hypothalamus, GP=Globus Pallidus, THAL=thalamus, AMYG=amygdala, HIPP=hippocampus, VTA/SN=ventral tegmental area/substantia nigra, STR=striatum, ALL=averaged subcortical correlation.

Although some subcortical regions display a positive *SST-PVALB* spatial correlation (e.g. striatum), anatomically defined regions do not always reflect functional organization[38]. For instance, the putamen contains subregions that differentially couple with default, frontoparietal, and somato/motor cortical functional networks[39]. Consequently, interneuron markers may show stereotyped patterns of expression when viewed through the lens of global functional network architecture rather than anatomy. Parallel distributed networks connect cortex, striatum, and thalamus to support complex affective, cognitive and motor behaviors[40]. To characterize relationships between these network boundaries and interneuron subtype organization, AHBA samples were aligned and analyzed according to functional parcellations of the striatum[39] and thalamus[41]. Suggesting that interneuron subtypes differentiate large-scale functional networks, paired-sample *t*-tests revealed significantly greater expression of *SST,* relative to *PVALB,* within a distributed limbic network encompassing ventral striatum (t(15)=6.08, p=2.1e-5), mediodorsal thalamus (t(72)=2.41, p=0.018; Figure 3c), and subgenual anterior cingulate and medial prefrontal cortex (mPFC; Figure 3e). Furthermore, we established that *SST*-biased sub-regions of the thalamus and striatum (Figure 3e-f) form a distributed functional network using resting-state data from an adult community-based sample (percent female=54.47, Age=62.66 (SD 7.45), min=45, max=80) from the UK Biobank project (N=9,627 see Supplemental Figures 3 & 4 for cortical correlations). Limbic striatum and default thalamus (Figure 3c) displayed overlapping positive functional connections (*r*'s>0.05) within medial prefrontal cortex (Figure 3e), an area with strong preferential expression of *SST* (*F*(1,337)=14.09, p=0.0002; Figure 3g). This mPFC-ventral striatum-mediodorsal thalamus network broadly supports reward and affective information processing and is consistently implicated in affective disorders[42].

Among regions of a distributed somato/motor network, relative *PVALB* expression was increased within sensory and motor cortex (Figure 3f) and dorsolateral putamen (t(11)=3.47, p=0.031), but not within ventrolateral thalamus (t(5)=1.22, p=0.28; Figure 3d), which may be due to particularly sparse sampling in this region (n=5). A visual medial occipital area of the thalamus also displayed preferential expression of *PVALB* (t(14)=2.74, p=0.016; Figure 3b), consistent with the proposal that *PVALB/SST* ratios are higher in distributed whole-brain networks that process visual and sensorimotor information[13]. Supporting this distinction, both somato/motor striatum and thalamus (Figure 3d) were positively functionally coupled (*r*'s>0.03) to motor and sensory cortex (Figure 3f), which show a *PVALB* expression bias (*F*(1,337)=6.86, p=0.009; Figure 3h).

Suggesting the *SST/PVALB* dissociation also extends to the midbrain, relative expression of *SST* (M=1.15 SD=0.52) was greater than that of *PVALB* (M=-0.24 SD=0.71) among ventral tegmental area (VTA) samples (t(12)=-7.17, p=1.1e-5), whereas *PVALB* (M=0.69 SD=0.88) was greater than *SST* (M=-0.13 SD=0.90) in the substantia nigra reticulata (STNr; t(23)=2.98, p=0.006; Supplemental Figure 2). The VTA is densely interconnected to other *SST*-biased regions, including the nucleus accumbens (NAcc), anterior cingulate cortex, and mediodorsal thalamus[42], whereas functional neuroimaging and tract-tracing work suggests the substantia nigra pars reticulata (SNr) preferentially functionally couples to motor areas and is reciprocally connected to sensorimotor striatum[40,43,44]. Together, these data suggest that *SST*

247 expression is greater within distributed limbic and affect-related regions, whereas *PVALB* expression is
248 elevated within a distributed sensorimotor processing network.

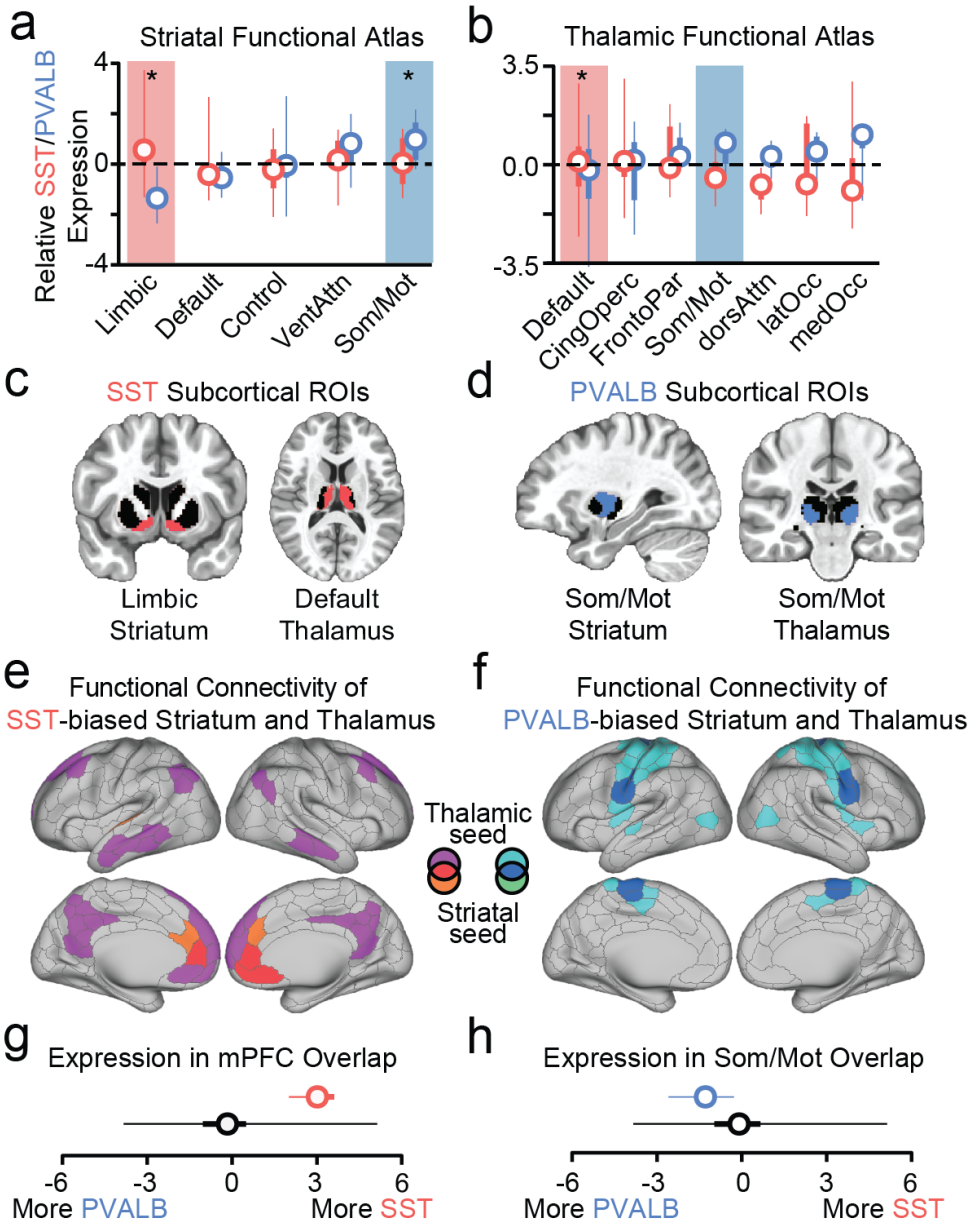

Figure 3. Differential *SST*/*PVALB* expression in distributed limbic and somato/motor networks. (a and b) Relative *SST* and *PVALB* expression across functionally defined striatal and thalamic subregions. (c) Relative expression of SST was highest within limbic striatum and default thalamus. (d) Relative PVALB expression was greater within somato/motor striatum and somato/motor thalamus. (e) Limbic striatum and default thalamus possess overlapping positive resting state correlations to *SST*-biased aspects of medial prefrontal cortex (mPFC; *r's*≥0.05). Likewise, (f) somato/motor striatum and thalamus show overlapping positive correlations to *PVALB*-biased portions of somatosensory cortex (*r's*≥0.03). (g) *SST* expression within the 3 overlapping mPFC limbic parcels is greater than all other cortical parcels. (h) *PVALB* expression within the 15 overlapping somato/motor parcels is greater than all other cortical parcels.

SST/_PVALB_ ratios co-vary with resting-state signal amplitude across cortex.

Computational work in rodents posits that the ratio of SST to PVALB interneurons contributes to regional differences in function and hierarchical organization across cortex[13]. Sensory and association cortices display hierarchically organized timescales of spiking activity that progress from shorter to longer, respectively[17,45]. This aspect of functional organization may be indexed by variability in the resting-state BOLD signal. Accordingly, we examined whether the ratio of cortical *SST*/*PVALB* expression relates to an *in-vivo* measurement of cortical signal variability, resting-state functional amplitude (RSFA)[46]. Voxel-wise RSFA was calculated using the UK Biobank sample (n=9,627) and averaged across the 400 parcel functional atlas of Schaefer and colleagues[47].

We first established the heritability of RSFA. Between-subjects hierarchical clustering was used to identify cortical territories with similar patterns of signal amplitude across individuals (Figure 4a), corresponding to limbic (light beige), cingulo-opercular (teal), temporo-parietal (orange), prefrontal (red), somato/motor (blue), and visual (purple) clusters. Consistent with recent work[48], this data-driven dimensionality reduction broadly categorized association and unimodal aspects of cortex. Suggesting that individual differences in RSFA can be explained by genetic variation in the general population, a significant proportion of between-subject variation in cluster-wise RSFA was found to be due to common genetic factors [h^2_{snp}: limbic=0.27 (SE 0.04), cingulo-opercular=0.22 (SE 0.04), temporo-parietal=0.28 (SE 0.04), prefrontal=0.31 (SE 0.04), somato/motor=0.21 (SE 0.04), visual=0.06 (SE 0.04)][49]. See Supplemental Figure 5 for parcel-wise estimates of RSFA heritability.

Expression data from the AHBA were used to test whether interneuron ratios track the spatial layout of RSFA signal variability across the cortical sheet. Earlier work has documented a correlation of interneurons marker expression with fractional Amplitude of Low-Frequency Fluctuations (fALFF)[50], a metric closely tied to RSFA, within a circumscribed set of cortical areas. Across the whole-brain Schaefer cortical parcellation, *SST*/*PVALB* ratio was negatively correlated with resting-state signal amplitude ($r(337)=-0.52$, $p\leq 2.2e-16$; Figure 4c. Parcels with higher relative expression of *SST* had lower RSFA (e.g. limbic parcels). Conversely, clusters with higher relative *PVALB* had higher RSFA (e.g., visual, parietal). Across individual interneuron markers, we observed a positive correlation to parcel-wise RSFA and expression of *PVALB* ($r=0.48$, $p\leq 2.2e-16$), and a negative correlation to *SST* ($r=-0.44$, $p\leq 2.2e-16$).

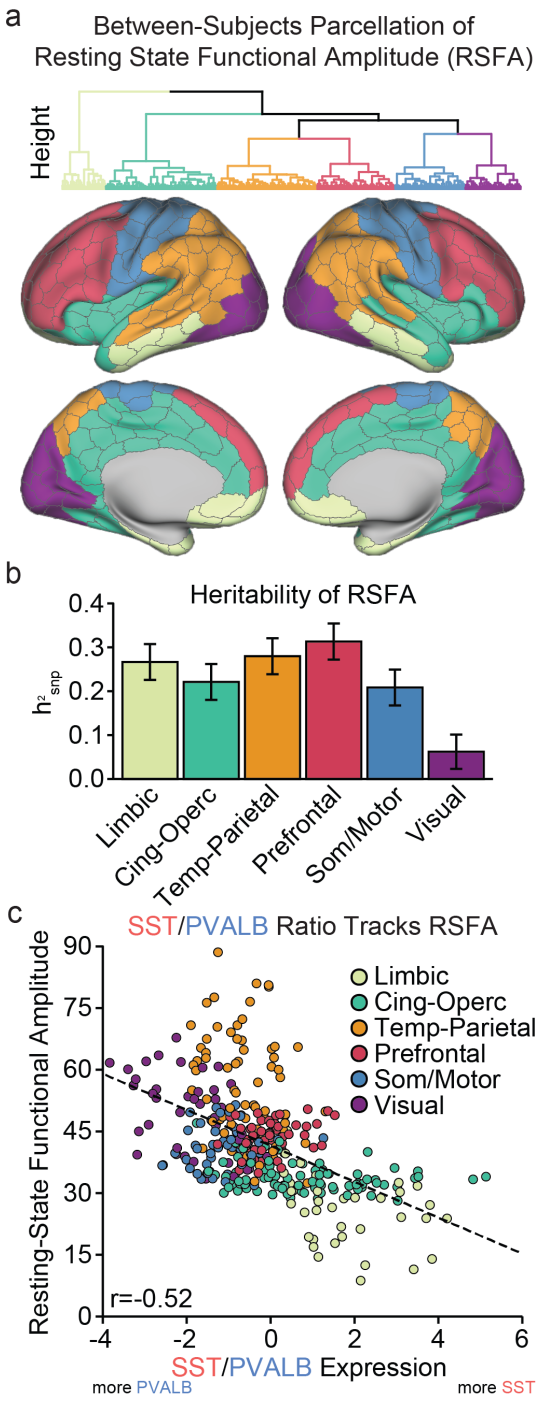

Figure 4. *SST/PVALB* ratio tracks inter-regional differences in cortical brain function. (a) Mean RSFA was calculated for each of 400 volumetric cortical parcels from the Schaefer parcellation[47]. Between-subjects hierarchical clustering of residualized RSFA values revealed 7-clusters of parcels with similar amplitude signatures; Light beige=limbic, teal=cingulo-opercular, orange=temporal-parietal, red=prefrontal, blue=somato/motor, and purple=visual. (b) Overall, a significant proportion of variability of RSFA was explained by common genetic variation (h^2_{SNP}=0.06-0.31; error bars=standard error) (c) Parcel-wise relative expression of *SST*/*PVALB* is negatively correlated to RSFA (r(337)=-0.52, p≤2.2e-16).

Polygenic variation among *PVALB*-correlated genes underlies cortical brain function

Genome-Wide Association Studies (GWAS) demonstrate that the genetic bases of many complex traits are due to the cumulative weight of genetic variants spread across the entire genome, each with a subtle effect[51]. Although brain phenotypes such as resting-state functional amplitude likely display such a polygenic architecture[52], phenotype-relevant polymorphisms can cluster in genes expressed within relevant tissue and cell types[53]. Given that cortical resting-state functional amplitude tracks the topography of interneuron ratios, we next tested whether single-nucleotide polymorphisms (SNPs) underlying the heritable variance in brain activity (i.e. RSFA) are enriched within genes linked to *PVALB* and *SST*. The observation that RSFA-related SNPs are enriched within interneuron-related genes would yield insight into the molecular basis of the resting-state BOLD fluctuations.

Interneuron-correlated gene sets were nominated using a guilt-by-association logic. That is, genes that were spatially correlated to interneuron markers (i.e. *SST, PVALB*) were assumed to relate to each interneuron subtype. Using cortical AHBA data, genes were rank-ordered based on their spatial correlation to each interneuron marker and the top 500 most-correlated genes were selected. *PVALB* and *SST* gene sets were non-overlapping. Interneuron-related SNP lists were generated for each gene set by identifying variants within ±5000 base pairs from transcription start and stop site of each gene. eQTL variants for each gene set were included, defined using cortical data from the CommonMind consortium[54] and NIH GTEx[55]. We denote the SNP lists for each interneuron gene set as $PVALB_{SNP}$ and SST_{SNP} (see Supplemental Data). Genetic relatedness matrices were calculated for the UKB sample using each SNP set, and heritability was estimated using GCTA-REML simultaneously across three partitions: $PVALB_{SNP}$, SST_{SNP}, and a partition containing all remaining genotyped variants[49].

Indicating that the genetic basis of RSFA, a measure of *in vivo* brain activity, is determined in part by genes linked to *PVALB* interneurons, the $PVALB_{SNP}$ set accounted for a significant proportion of heritable variance of the temporo-parietal (h^2_{PVALB}=0.029 ,SE=0.0092, q=0.0047), prefrontal (h^2_{PVALB}=0.023, SE=0.0091, q=0.016), and somato/motor (h^2_{PVALB}=0.019, SE=0.0087, q=0.034) RSFA clusters, but not the limbic (h^2_{PVALB}=0.006, SE=0.008, q=0.25), cingulo-opercular (h^2_{PVALB}=0.006, SE=0.0082, q=0.25), or visual (h^2_{PVALB}=0.012, SE=0.008, q=0.11) clusters. Conversely, the SST_{SNP} set did not explain a significant proportion of heritable variance across any partition (h^2_{SST}s<0.0075, ps>0.46). A key question is whether the genetic variance explained by the $PVALB_{SNP}$ set is greater than what is expected given the number of SNPs examined, which would indicate the outsized, or enriched, role of these genetic variants in RSFA. Enrichment was calculated as the proportion of heritability explained by the partition, divided by the fraction of SNPs in that partition, where a value greater than 1 denotes enrichment. We observed fold enrichment greater than 1 for visual (enrich=6.49 SE=0.28), motor (enrich=3.02 SE=0.30), temporo-parietal (enrich=3.64 SE=0.32), prefrontal (enrich=2.53 SE=0.31) clusters, but not limbic (enrich=0.76 SE=0.29) or cingulo-opercular (enrich=0.86 SE=0.28). The $PVALB_{SNP}$ list (N=9,819 variants) constituted 2.9% of total analyzable genotyped SNPs (N=337,356 variants), but accounted for 2.2-18.9% (M=8.4 SD=6.1) of total genetic variance across each of the RSFA

clusters (Figure 5a). The SST_{SNP} partition (2.6% of available variants) did not explain a significant proportion of genetic variance for any RSFA cluster.

An important unanswered question is whether the genetic determinants of RSFA are uniform across cortex, or whether they vary according to underlying cytoarchitecture. We next tested whether the $PVALB_{SNP}$ and SST_{SNP} partitions explain a greater percentage of heritable RSFA variance in regions where the respective marker is expressed most. Partitioned heritability analyses were performed for each of the 400 Schaefer cortical parcels. Across all parcels with available AHBA expression data, normalized genetic variance explained by the $PVALB_{SNP}$ partition was positively correlated to *PVALB* expression (Figure 5b; $r(326)=0.36$, p=1.78e-11), corresponding to visual, superior temporal, and parietal areas of cortex (Figure 5b). Across all genes, *PVALB* was among the top 64 transcripts (top 0.003% of 20,738 transcripts) showing a positive spatial correlation to the $PVALB_{SNP}$ partition map (i.e. Figure 5b), indicating that this positive relationship is not obligated by global statistical properties. Conversely, partitioned $PVALB_{SNP}$ heritability was negatively correlated to *SST* expression ($r(326)=-0.36$, p=2.85e-11). There was not a significant parcel-wise relationship between SST_{SNP} partitioned heritability and SST gene expression ($r(326)=-0.03$, p=0.54). Together, these findings indicate that the molecular genetic basis of resting-state functional amplitude is spatially heterogeneous, demonstrating a particularly important role of genes co-expressed with *PVALB*.

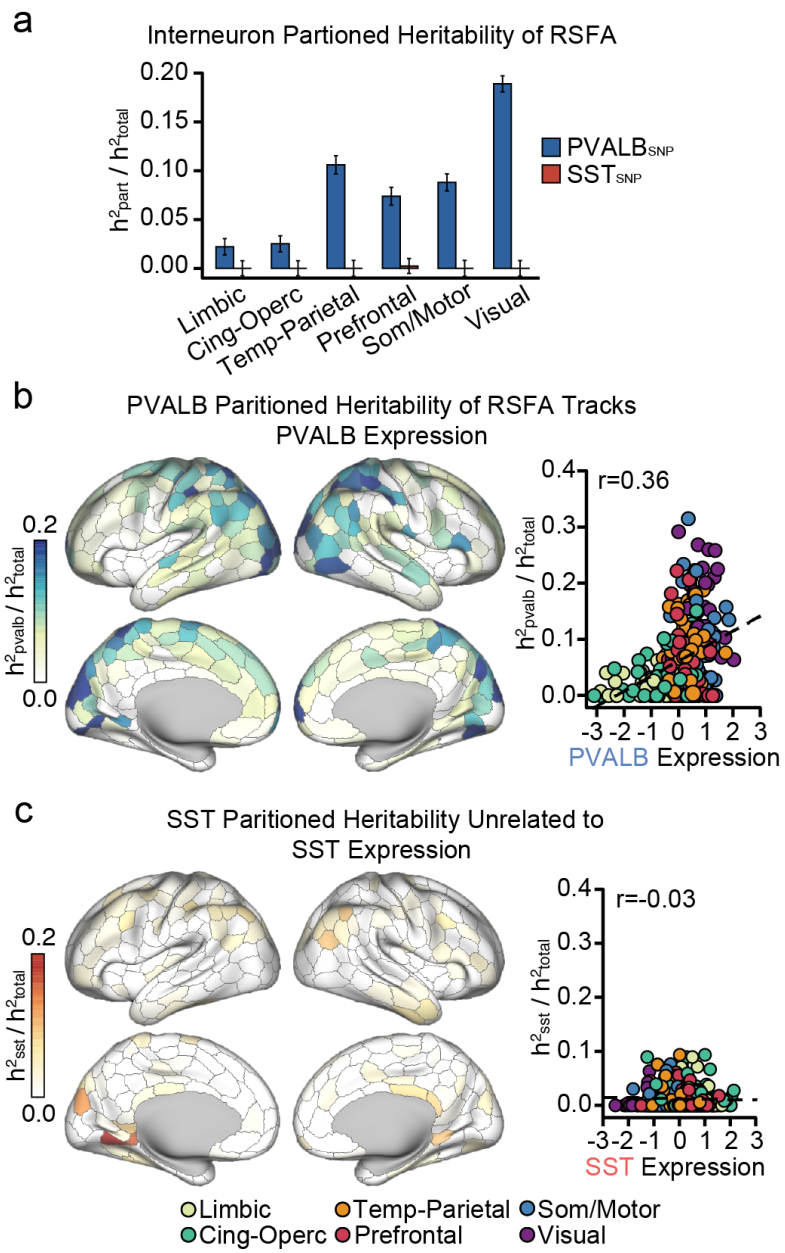

Figure 5. *PVALB* genes underlie spatially variable patterns of heritable brain function. (a) Across the six data-defined RSFA clusters, the 500 gene PVALB$_{SNP}$ set accounted for a significant proportion of heritable variance in cingulo-opercular, prefrontal, and temporo-parietal areas. PVALB$_{SNP}$ enrichment was observed within tempero-parietal, prefrontal, som/motor, and visual clusters. (b) Parcel-wise partitioned heritability tracks sub-type specific gene expression for PVALB$_{SNP}$ (r(326)=0.36, p=1.78e-11), (c) but not the SST$_{SNP}$ (r(326)=-0.03, p=0.54), partitions. Error bars=SE.

The association between genetic risk for schizophrenia and brain function follows the spatial profile of *PVALB* expression

Understanding the molecular genetic underpinnings of brain function is pressing given the need for empirically informed treatment targets for heritable, brain-based, psychiatric illnesses like schizophrenia[56]. Convergent evidence from animal models and post-mortem tissue analyses suggests that interneuron dysfunction as a core pathophysiological feature of schizophrenia[57]. To determine whether interneuron-related genetic variation is tied to disease liability, we tested whether polygenic risk for schizophrenia[58] is greater among $PVALB_{SNP}$ and SST_{SNP} variants, relative to the rest of the genome. Using a partitioned MAGMA analysis[59], we divided rank-ordered *PVALB,* and *SST* gene lists into bins of 500. Using MAGMA, we observed significant enrichment of schizophrenia polygenic risk for the top *PVALB* gene set (beta=0.083, p=0.038), but not the top *SST* (beta=-0.01, p=0.61). Suggesting that polygenic schizophrenia risk is greater among interneuron-related genes, we examined all gene bins examined and found that the enrichment of schizophrenia genetic risk decreased as gene bins became less spatially correlated with *PVALB* ($r(18)$=-0.65, p=0.0017), but not *SST* ($r(18)$=-0.39, p=0.09; Figure 6a).

To test whether polygenic risk for schizophrenia influences cortical RSFA, we calculated a schizophrenia polygenic risk score (SCZ-PRS)[60] using genotyped variants from individuals in the UK Biobank imaging sample. Across the data-derived RSFA clusters, SCZ-PRS negatively predicted RSFA in the visual cluster (Benjamini-Hochberg corrected q=0.016; Figure 6b; GWAS threshold p<1.0), as well as somato/motor (q=0.070) and prefrontal (q=0.097) clusters at trend-levels. Consistent with the hypothesized link between PVALB interneurons and psychotic illness, the relationship between RSFA and polygenic schizophrenia risk was significantly negatively correlated to the topography of *PVALB* expression across cortex ($r(337)$=-0.43, p≤2.2e-16; Figure 6c). That is, regions where SCZ-PRS most negatively predicted RSFA corresponded to areas with the greatest *PVALB* expression (e.g. motor and visual parcels). This relationship remained significant after controlling for the overall SNP-wise heritability of each parcel (β=-.38, $t(336)$=-7.48, p=6.73e-13), indicating that the effect is independent of parcel-wise explainable genetic variance. Comparing the RSFA-schizophrenia polygenic risk map to all genes, *PVALB* was the among the top 0.0034% negatively correlated expression profiles (72 out of 20,738), showing that this relationship is not obligated by globally negative relationships between gene expression and schizophrenia risk RSFA effects. Ontological enrichment analysis further revealed that the top 500 genes correlated with *PVALB* in the AHBA data contained genes associated to schizophrenia and bipolar disorder, neuronal signaling, and gated channel activity (Table 1). Together, these data suggest that schizophrenia-related genetic variants cluster within cell types, particularly parvalbumin interneurons, leading to differential functional disruption across cortex.

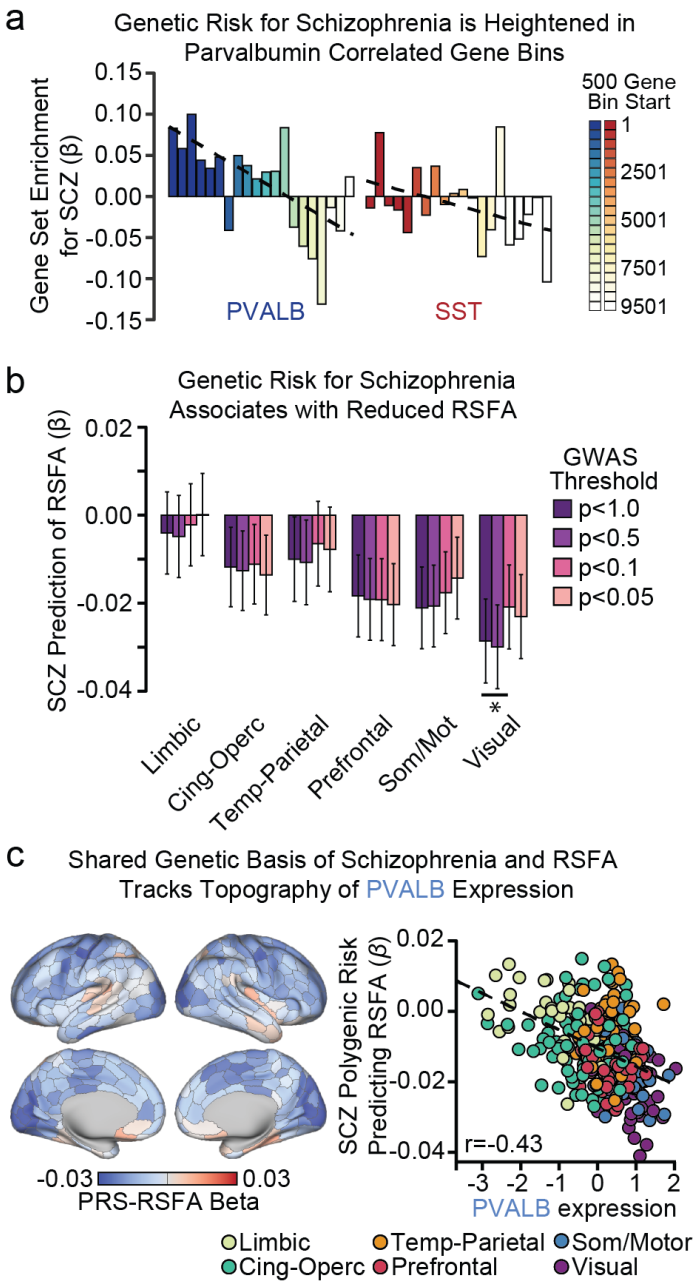

Figure 6. Schizophrenia polygenic risk predicts brain function and tracks *PVALB* expression. (a) Genes were rank-ordered by cortical spatial correlation to *SST* and *PVALB,* then divided into 500 gene bins. MAGMA competitive gene set analysis revealed enrichment of polygenic risk for schizophrenia in the top *PVALB* (p=0.032), but not the top *SST* (p=0.62) set. Enrichment decreased across ordered bins for *PVALB* (r=-0.65, p=0.0017) and *SST* (r=-0.39, p=0.09). (b) Schizophrenia polygenic risk negatively predicts RSFA within the visual (q=0.016) cluster, as well as somato/motor (q=0.070) and prefrontal (q=0.097) clusters at trend-levels. (f) Parcel-wise prediction of RSFA by the schizophrenia PRS significantly negatively correlated with cortical expression of *PVALB* (r=-0.43, p=2.2e-16). SCZ=schizophrenia; PRS=Polygenic Risk Score; RSFA=Resting State Functional Amplitude. *=q≤0.05.

	Category	ID	Name	p	q FDR-BH	Hits	Genes in GO
SST	GO: BP	GO:0099536	synaptic signaling	1.08e-5	2.16e-2	37	687
	GO: BP	GO:0099537	trans-synaptic signaling	1.95e-5	2.16e-2	36	678
	GO: CC	GO:0097458	neuron part	3.35e-6	6.31e-4	68	1545
	GO: CC	GO:0045202	synapse	3.3e-4	1.69e-2	39	870
PVALB	GO: MF	GO:0005261	cation channel activity	3.33e-12	1.74e-9	33	306
	GO: MF	GO:0005249	voltage-gated potassium channel activity	1.33e-10	1.69e-8	17	91
	GO: BP	GO:0071805	potassium ion transmembrane transport	2.75e-10	6.61e-7	23	181
	GO: BP	GO:0098655	cation transmembrane transport	9.85e-9	7.88e-6	47	738
	GO: CC	GO:0034703	cation channel complex	1.04e-10	5.07e-8	23	176
	GO: CC	GO:0034702	ion channel complex	3.03e-10	5.07e-8	29	291
	Disease	C0036341	Schizophrenia	1.93e-7	7.27e-4	70	1561

Table 1. Enrichment terms for interneuron-correlated genes. Ontological enrichment analyses were conducted with ToppGene on the 500 genes used to generate the $PVALB_{SNP}$ and SST_{SNP} lists.

Discussion

Integrating genetic, transcriptional, and neuroimaging data, we demonstrate that spatial distributions of interneurons are stereotyped across species and development, align to the topographic distribution of functional brain networks, and underlie a substantial portion of the heritable aspects of resting-state functional amplitude, a measure of *in vivo* brain activity. Somatostatin- and parvalbumin-interneuron markers were negatively spatially correlated across cortex, a relationship that was robust in early developmental periods in humans and evolutionarily conserved in non-human primates (Figure 1). Stereotyped patterns of *SST* and *PVALB* expression were observed in subcortex (Figure 2), with *SST* and *PVALB* differentially expressed within distinct limbic and somato/motor functional networks linking cortex, striatum, and thalamus (Figure 3), respectively. Computational models theorize that interneuron ratios underlie regional differences in cortical brain function[13]. Providing empirical support for this hypothesis, regional differences in *SST/PVALB* expression in post-mortem brain tissue align with spatial variability in resting-state functional amplitude in the general population (Figure 4). Suggesting the functional relevance of this spatial relationship, genetic polymorphisms linked to PVALB interneurons accounted for an enriched proportion of heritable variance underling cortical signal amplitude (Figure 5). Critically, the amount of variance explained by *PVALB* SNPs positively tracked spatial expression of *PVALB*, suggesting that common genetic polymorphisms influence brain function in a cell-type specific and regionally variable manner. Implicating genetic differences among interneurons in schizophrenia, schizophrenia-related polygenic risk was enriched among genes co-expressed with interneurons, and predicted reduced resting-state functional amplitude across cortex in a manner that tracked the spatial landscape of *PVALB* gene expression (Figure 6).

Adaptive functioning depends on the brain's capacity to integrate information across timescales. Higher-order cognition often requires information accumulation over time, whereas sensorimotor processing entails rapid adaption to changing external stimuli[18,47,65,66]. These informational demands are met, in part, through the hierarchical organization of anatomic and functional connections in cortex, as well cytoarchitectural gradients that underlie regional specialization[12,61]. Our data indicate that interneuron ratios, as indexed by *SST* and *PVALB* expression, are an important feature underlying regional differences in brain function (Figure 4). Due to unique electrical and synaptic properties of somatostatin and parvalbumin interneurons, relative shifts in their density can alter the balance of inhibitory control[13]. SST interneurons synapse onto dendrites of pyramidal neurons to gate incoming cortical signals, whereas PVALB interneurons provide perisomatic inhibition that is well-suited for feedback inhibition and output regulation[2]. Computational models suggest that increased dendritic (i.e. SST) over perisomatic (i.e. PVALB) inhibition results in more robust filtering of distracting information, allowing for greater recurrent excitation in association cortex for complex tasks requiring integration of information over time[20]. Conversely, sensorimotor regions may benefit from fast responses and lower recurrent excitation to adapt to rapidly changing inputs[17], which could be facilitated by direct inhibitory signals from parvalbumin-expression interneurons.

Our analyses provide molecular genetic support for a relationship between parvalbumin interneurons and the hemodynamic BOLD signal. A wealth of evidence indicates that BOLD signal most tightly couples to gamma oscillations (30-80 Hz) relative to other frequency domains[21-25]. Individual differences of GABA in visual cortex predict both gamma oscillations and BOLD amplitude[62], a relationship that animal work suggests is primarily driven by parvalbumin interneurons[19]. Here, we provide initial evidence in humans for the preferential influence of parvalbumin interneurons on fMRI signal. For instance, polygenic variation among parvalbumin correlated genes explained upwards of 18% of the heritable variance in RSFA in visual cortex.

Schizophrenia is among the most heritable forms of psychiatric illness (h^2=81%)[63], underscoring the pressing need to map polygenic variation to illness-related brain phenotypes and associated risk factors. Converging lines of evidence point to GABAergic abnormalities as a cardinal feature of the disorder[64], highlighting a particular role of parvalbumin interneurons[26]. Patients with schizophrenia exhibit reduced levels of GAD67, an enzymatic precursor of GABA[65], and are characterized by parvalbumin interneurons with atypical perineuronal nets[66], dysregulated mitochondrial gene transcription[67], and reduced potassium signaling channels[68] relative to healthy populations. These abnormalities are thought to underlie disrupted gamma-band oscillations and working memory deficits which are a hallmark of the disorder[64]. Linking these observations, we demonstrate here that polygenic risk for schizophrenia is increased among genes that are spatially correlated to *PVALB* (Figure 6a), expanding upon cell transcriptomic work implicating cortical interneurons as an illness marker[53]. Consistent with a relationship between schizophrenia-linked genetic vulnerability and brain function, we document a negative association between individual polygenic schizophrenia risk and resting-state functional amplitude in a large population-based sample (Figure 6b). Importantly, the topography of these effects follows spatial profile of *PVALB* expression across cortex (Figure 6c), highlighting the potential role of parvalbumin interneurons in mediating brain-based intermediate phenotypes associated with illness risk.

Disruption of excitatory/inhibitory balance is thought to reflect a cross-diagnostic marker of psychiatric illness[69]. For instance, decreased expression of parvalbumin cell markers is evident in both schizophrenia and bipolar disorder[70], while major depressive disorder (MDD) is marked by selective reductions in somatostatin interneurons[71]. Delineating the region-specific functional roles of cortical interneuron subtypes will provide biological insight into cross-diagnostic patterns of both behavior and brain function. With regard to depressed mood and negative affect, modulation of cortical somatostatin interneurons can causally influence anxiety- and depressive-like behavioral phenotypes in rodents[7,72]. In line with this observation, we observe the greatest expression of somatostatin within a distributed limbic network linking mPFC, NAcc, and mediodorsal thalamus (Figure 3) that processes reward and affective information[42]. Somatostatin-biased cortical regions (ACC, mPFC, and insula) also correspond to areas where cortical thinning has been observed in patients with MDD[73,74] and individuals reporting elevated negative affect[75]. These converging lines of evidence support the hypothesized role of somatostatin

477 neurons in mood-related psychiatric symptoms[71], which should be explored in future work on the
478 molecular and neural underpinnings of affective illness.
479 The present findings should be interpreted in light of several limitations. First, we use single
480 molecular markers to infer the relative presence of SST and PVALB interneurons, which are not sensitive
481 to morphological and physiological differences among interneuron subgroups[2]. More nuanced inference
482 of cellular spatial distributions should be conducted as single-cell transcriptomic atlases are developed in
483 humans. Further, we employ a "guilt-by-association" logic to nominate interneuron related gene sets.
484 While we cannot conclude that genes within each identified interneuron group directly influence
485 interneuron function, similar correlation-based nomination approaches have been shown to correspond
486 well with *a priori* defined gene groups[76]. The examination of enrichment terms (Table 1; Supplemental
487 Information) allows for more precise understanding of the biological processes contributing to our results.
488 Lastly, the *in vivo* imaging and genetic analyses focus on an aging population of White/non-Latino
489 individuals. As genetic effects can vary across ethnic and demographic subgroups[77,78], the stability of the
490 results reported here should be examined across diverse populations.
491 Inherited genetic variation shapes brain function within and across individuals[79,80]. There is
492 pressing need to identify specific molecular genetic mechanisms of human brain function to expand our
493 biological understanding of cognition, behavior, and associated risk for psychiatric illness. Analyses of
494 spatially-dense, whole-genome, expression atlases increasingly reveal transcriptional correlates of brain
495 function[50], structure[12,87-89], functional connectivity[8-10], and psychiatric illness[81]. With the emergence of
496 large-scale imaging genetic data[27], it is now possible to bridge structural genetic, transcriptional, and
497 large-scale neuroimaging brain phenotypes. Here, we leverage these data to show that interneuron
498 marker distributions correlate with cortical signal amplitude, align to distributed functional networks,
499 underlie regional differences in heritable brain function, and associate with genetic risk for schizophrenia
500 in the general population.

Methods

Allen Human Brain Atlas.

Publicly available human gene expression data from six postmortem donors (1 female), aged 24–57 years of age (42.5±13.38) were obtained from the Allen Institute[33]. Data reflect the microarray normalization pipeline implemented in March 2013 (http://human.brain-map.org) and analyses were conducted according to the guidelines of the Yale University Human Subjects Committee. Microarray probes from eight overarching ontological categories were selected: cortex, dorsal thalamus, striatum, globus pallidus, hypothalamus, hippocampus proper (i.e. CA1-CA4), amygdala, and the combined substantia nigra and ventral tegmentum (see Supplemental Information). For genes with duplicate probes, the *collapseRows* function[82] was used in R to select the probe with the highest mean expression (connectivityBasedCollapsing=FALSE), resulting in 20,738 unique mRNA probes. ComBat was used to normalize expression across donors before combining data from each brain[83].

Individual cortical tissue samples were mapped to each AHBA donor's Freesurfer derived cortical surfaces, downloaded from Romero-Garcia and colleagues[84]. Native space midthickness surfaces were transformed to a common fsLR32k group space while maintaining the native cortical geometry of each individual donor. The native voxel coordinate of each tissue sample was mapped to the closest surface vertex using tools from the HCP workbench[85]. Microarray expression of each gene was mean- and variance-normalized (i.e., divided by standard deviation) separately for each of the eight analyzed regions, revealing relative expression differences within cortical and subcortical territories. For region-wise expression analyses (e.g. Figure 1c), ontological categories from the AHBA were used to calculate the median, min-max, and interquartile range of relative expression in each region. Detailed information about the analyzed regions is provided in the Supplemental Information. Cortical data visualization was carried out using *wb_view* from the HCP workbench[85]. The MNI locations of striatal and thalamic samples were cross-referenced to functional atlases of Choi and colleagues[39] and Hwang and colleagues[41]. With AFNI, a single voxel (1 mm^3) region of interest (ROI) was generated at the MNI location of each sample. A functional network label was assigned if the ROI fell within a volumetric parcel. If the sample did not overlap with the functional atlas, the associated ROI was expanded to 2 mm^3 and the network with the most overlapping voxels in the ROI was assigned. If the expanded 2 mm^3 ROI did not overlap, the process was repeated using a 3 mm^3 ROI. A sample was omitted from analysis if the 3 mm^3 ROI did not overlap with the associated functional atlas. Functional sub-regions with 3 or fewer samples were excluded from analyses.

UKB imaging processing

Minimally preprocessed resting-state fMRI data from the UK Biobank were analyzed, reflecting the following preprocessing steps: motion correction with MCFLIRT[86], grand-mean intensity normalization, highpass temporal filtering, fieldmap unwarping, and gradient distortion correction. Noise terms were identified and removed using FSL ICA+FIX[87]. Full information on the UKB preprocessing is published[27].

Additional processing was conducted in AFNI[88] and consisted of 3dDespike, resampling to MNI152 space using the UKB generated linear and nonlinear transforms, FWHM blur of 4.0mm, regression of CSF,WM, and global resting state signals, and first and second order trend removal. Voxel-wise RSFA maps were generated with 3dRSFC and then averaged within each of the approximately symmetrical 400 volumetric parcels from the 7-Network parcellation of Schaefer and colleagues[47]. Due to signal blurring between lateral striatum and insular cortex, resting-state analyses reflect an additional local white-matter regression against gray matter using AFNI anaticor. Imaging analyses were conducted in volume, but visualized on the cortical surface. Resting-state functional connectivity between striatum, thalamus, and cortex was estimated using AFNI's 3dNetCorr, which calculated the Fisher-Z transformed correlation values of timeseries across the Choi 7-region striatal atlas[39], the Hwang 9-region thalamic atlas[41], and the Schaefer 400-region cortical atlas[47].

A total of 13,236 UKB subjects were processed through the imaging pipeline. Subjects with mean run-wise frame-to-frame head motion greater than 0.20mm, and inverted rsfMRI SNR greater than 3 standard deviations above the mean were removed. After filtering for White/Non-Latino subjects with usable genetic data, cryptic relatedness <0.025, and conducting row-wise deletion for the variables age, sex, height, weight, BMI, combined gray/white matter volume, combined ventricular/CSF volume, diastolic and systolic blood pressure, run-wise rsfMRI motion, rsfMRI inverse SNR, T1 inverse SNR, and UK Biobank assessment center, 9,627 subjects remained for analyses (percent female=54.47, mean age=63.33 SD=7.45, min/max age=45-80).

UKB genetics

UK Biobank genotype data was filtered to include only White/Non-Latino subjects with imaging data passing the quality control thresholds described above. Plink v2.00 was used to remove samples with missingness >0.10, SNPs with minor-allele frequency <0.05, Hardy-Weinberg equilibrium $<1x10^{-6}$, and call rate <0.02, resulting in 337,356 autosomal variants[89]. GCTA software was used to calculate a genetic relatedness matrix to remove individuals with cryptic relatedness more than 0.025, leaving N=9,627 subjects for analysis[49]. Ten genetic principal components were then calculated for use as covariates in polygenic risk score and heritability analyses.

RSFA between-subjects clustering and heritability

Voxel-wise RSFA data from the (N=9,627) UK Biobank sample was averaged within each of 400 roughly symmetric volumetric ROIs from the 7-Network cortical parcellation of Schaefer and colleagues[47]. Parcel-wise RSFA values were residualized for the effect of age, sex, age^2, ageXsex, age^2Xsex, height, weight, BMI, combined gray/white matter volume (normed for head size), combined ventricular/CSF volume (normed for head size), diastolic and systolic blood pressure, run-wise rsfMRI motion, rsfMRI inverse SNR, T1 inverse SNR, and UK Biobank assessment center. Hierarchical clustering of residualized RSFA estimates was conducted using R in order to group regions with similar between-subject patterns

of covariation. A 6-parcel RSFA clustering solution was selected. Raw RSFA values were then averaged across parcels falling within the same data-derived between-subjects cluster for use in heritability analyses. SNP-wise heritability of RSFA was estimated with genotyped data using GCTA-REML software. Age, sex, age^2, height, weight, BMI, combined normed gray/white matter volume, combined normed ventricular/CSF volume, diastolic and systolic blood pressure, run-wise rsfMRI motion, rsfMRI inverse SNR, T1 inverse SNR, UK Biobank assessment center, and 10 genetic principal components were included as covariates.

Partitioned heritability analyses were conducted for the six RSFA clusters and for each of the 400 individual cortical parcels. Using AHBA expression data, genes were rank ordered by their spatial cortical correlation to *SST* and *PVALB*. Genes without Entrez IDs were removed. The BioMart package[90] was used to identify each gene's transcription start and stop sites (±5000 base pairs) according to the GRCh37-hg19 genome assembly. If no UKB genotyped variants fell within the intragenic regions of a particular gene, that gene was excluded from analyses. Otherwise, the gene was cross-referenced to cortical eQTL databases from the NIH GTEx project[55] and CommonMind consortium[54]. Intragenic (±5000 base pairs) and eQTL SNPs associated with the top 500 *SST* (N_{SNP}=8,612) and *PVALB* (N_{SNP}=9,819) correlated genes were used for partitioned heritability analyses, respectively denoted SST_{SNP} and $PVALB_{SNP}$. Genetic-relatedness matrices for the SST_{SNP} and $PVALB_{SNP}$ partitions were generated, as well as one for all remaining genotyped SNPs. RSFA heritability accounted for by each genetic relatedness matrix was estimated simultaneously for each of the three partitions using GCTA[49]. Partitioned heritability was then defined as the ratio phenotypic variance explained by either the SST_{SNP} or $PVALB_{SNP}$, divided by the total phenotypic variance. To calculate the significance of individual partitions, we consider the Wald test statistic against the null of $h^2_{part} = 0$, which follows a half-half mixture of χ^2_0 (a χ^2 distribution with a probability mass at zero) and χ^2_1 (a χ^2 distribution with 1 degree of freedom). Enrichment values were calculated to determine if the proportion of variability explained by a partition was greater than the proportion of variants within the partition, defined as:

$$enrich_{part} = \frac{(h^2_{part} / h^2_{total})}{(g_{part} / g_{total})}$$

where h^2_{part} is the heritable variance explained by the SNP partition (e.g. $PVALB_{SNP}$), h^2_{total} is the heritable variance explained by all partitions, g_{part} is the number of variants within the SNP partition, and g_{total} is the total number of genotyped SNPs. Standard error for SNP partitions were similarly scaled by the genome partition denominator. When calculating RSFA partitioned heritability across individual parcels (i.e. Figure 5), parcels with outlier partitioned heritability (i.e. $PVALB_{PART}$, SST_{PART}) and expression (i.e. *PVALB, SST*) greater than 4 standard deviations from the mean were excluding, resulting in 328 observations across cortex.

To assess whether schizophrenia polygenic risk was enriched among *SST* and *PVALB* correlated gene sets, competitive gene-set analysis was conducted using MAGMA[59]. Rank-ordered *SST* and *PVALB* genes were divided into twenty non-overlapping 500-gene bins. Schizophrenia summary statistics from

611 the GWAS of Ripke and colleagues was used[58]. Intragenic variants were defined using a ±5000 base pair
612 window, and gene set enrichment was estimated simultaneously across all 40 gene bins, revealing
613 whether a particular bin is more associated with polygenic risk for schizophrenia than all other genes.
614 Polygenic risk for schizophrenia[58] was calculated using PRSice[60]. Only the top-SNP from the major
615 histocompatibility complex was used for generation of individual risk scores. Benjamani-Hochberg False-
616 discovery rate correction was conducted separately for each GWAS p-value threshold examined (e.g.
617 correction for 6 tests at the GWAS p<1.0 threshold).
618
619 **NIH Blueprint processing**
620 Publicly available microarray data from six adult macaque primates (3 Female) were downloaded
621 from the Gene Expression Omnibus website (https://www.ncbi.nlm.nih.gov/geo; accession number
622 GSE31613). Expression values were converted from log10 to log2. Data from two macaques (1 Female)
623 were excluded due to sparse sampling across cortex. Samples from the following 10 cortical regions were
624 included in our analyses: OFC, ACC, medial temporal lobe, temporal area, DLPFC, A1C, S1C, M1C, V1,
625 and V2. The *collapseRows* function[82] was used in R to select the probe with the highest mean expression
626 and ComBat was used to remove residual donor effects. *SST* and *PVALB* expression were mean and
627 variance-normalized to reveal relative expression differences across cortex.
628
629 **BrainSpan processing**
630 Publicly available RNAseq reads per kilobase per million (RPKM) data from the Brainspan atlas
631 were used to characterize patterns of interneuron-marker gene expression across development. Cortical
632 tissue samples were analyzed from early fetal [8-12 post-conception weeks (pcw), N=10, samples=88],
633 early/mid fetal (13-21 pcw, N=10, samples=88), late fetal (24-37 pcw; N=5, samples=27), early infancy (4
634 months; N=3, samples=22), late infancy (10 months; N=1, samples=8), early childhood (1-4 yrs; N=5,
635 samples=41), mid/late childhood (8-11 yrs; N=2, samples=30), adolescence (13-15 yrs; N=2,
636 samples=14), and adulthood (18-40 yrs; N=8, samples=85) developmental. RNAseq probes without
637 entrez IDs were excluded and duplicated probes were removed by selecting the probe with the highest
638 mean expression. Data was log2 transformed and the effect of donor was removed separately for each
639 age group using ComBat. Gene expression was then mean- and variance-normalized across cortical
640 tissue samples separately for each developmental stage. When multiple ages were present in a
641 development stage, age was included as a covariate in a linear regression predicting normalized *SST*
642 expression from normalized *PVALB* expression.
643
644 **Code Availability**
645 Code used for these analyses will be made available upon publication at the following url:
646 https://github.com/HolmesLab/Anderson2019_interneuron

SUPPLEMENTAL FIGURES

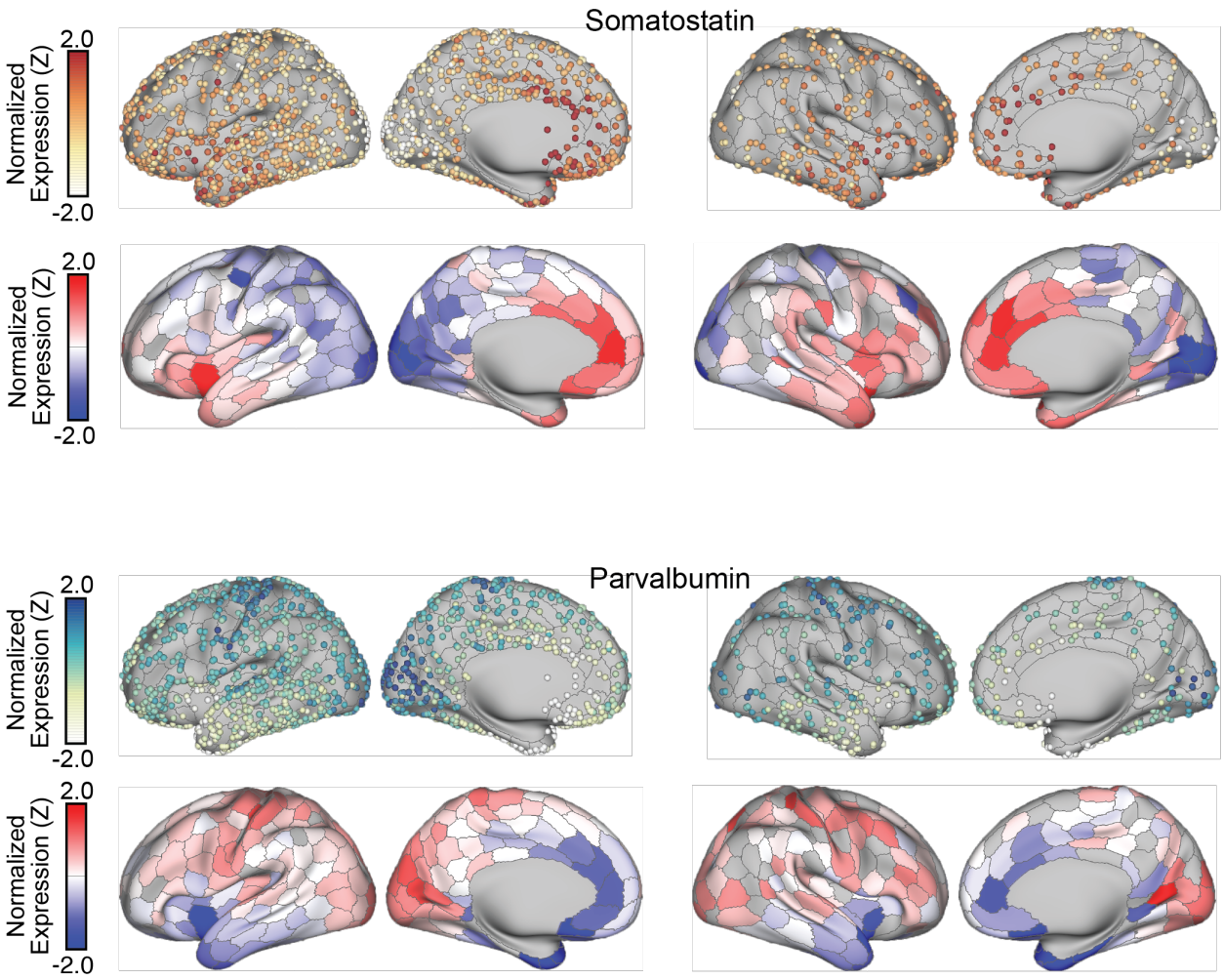

Supplemental Figure 1. Sample and parcel-wise expression of interneuron markers *SST* and *PVALB*.

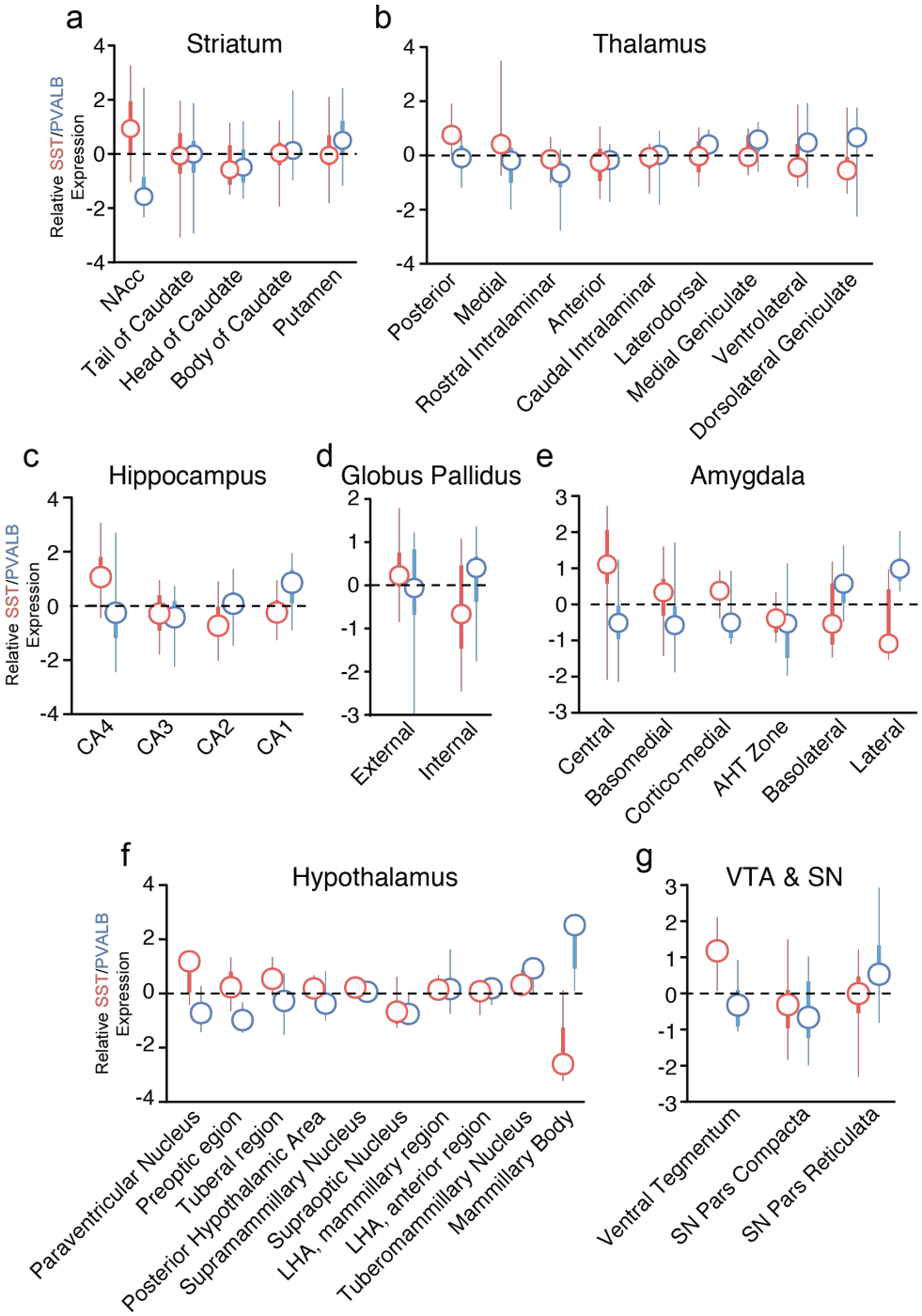

Supplemental Figure 2. Z-transformed expression values of SST and PVALB for subregions of (a) striatum, (b) thalamus, (c) hippocampus, (d) globus pallidus, (e) amygdala, (f) hypothalamus, and (g) combined ventral tegmentum and substantia nigra. Regions are ordered by relative median expression of SST to PVALB. Circle=median, thick lines=interquartile range, thin line=minimum and maximum.

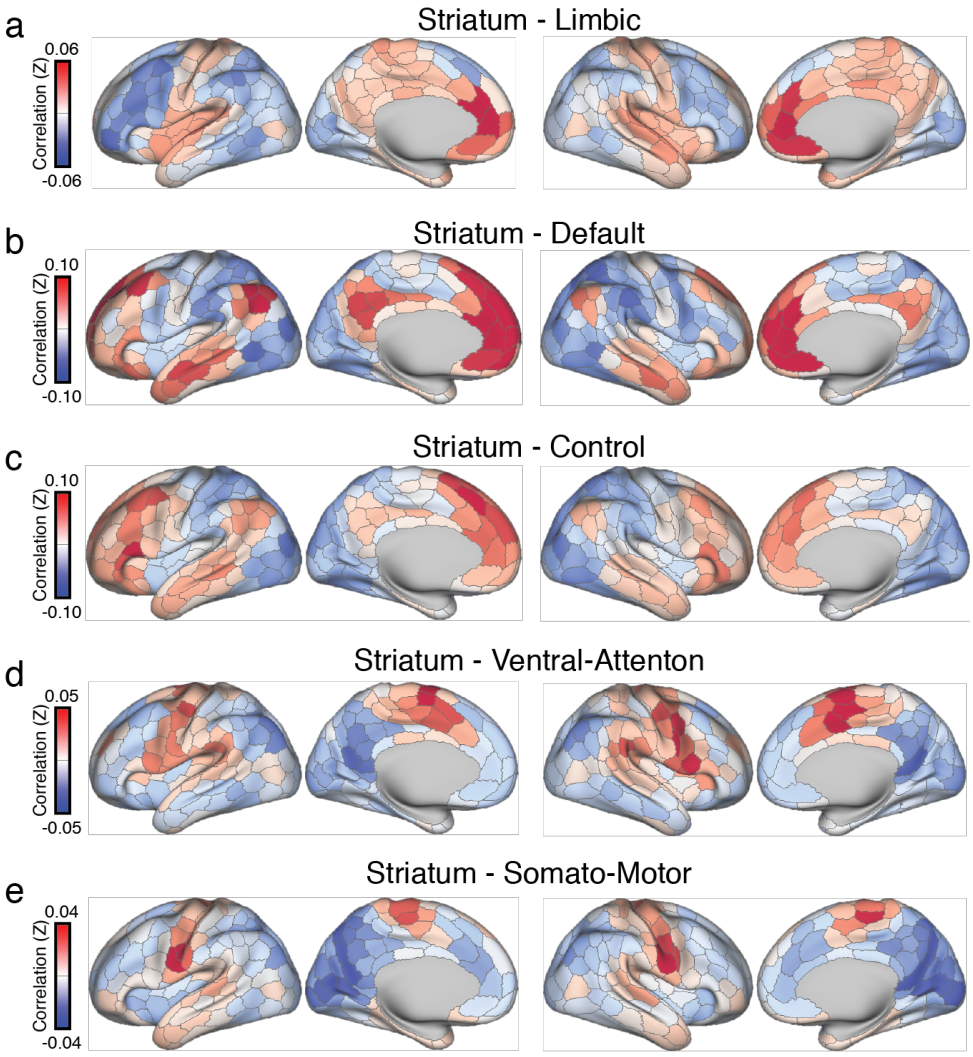

Supplemental Figure 3. Cortical resting-state functional correlation profile for each of the 5 striatal parcels[39] with analyzable AHBA expression data. Averaged maps were calculated using data from 9,627 participants from the UK Biobank.

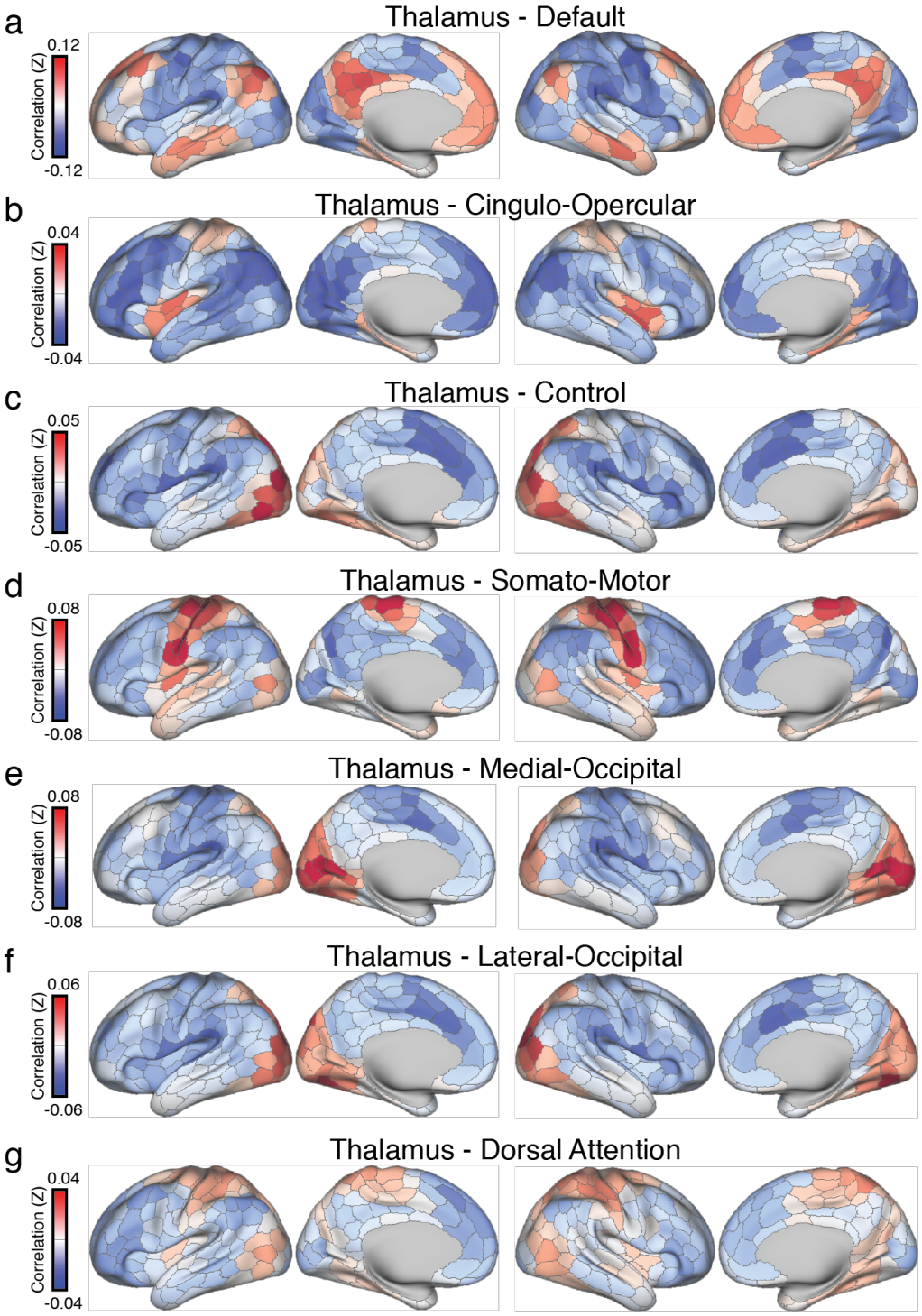

Supplemental Figure 4. Cortical resting-state functional correlation profile for each of the 6 thalamic parcels with analyzable AHBA expression data[41]. Averaged maps were calculated using data from 9,627 participants from the UK Biobank.

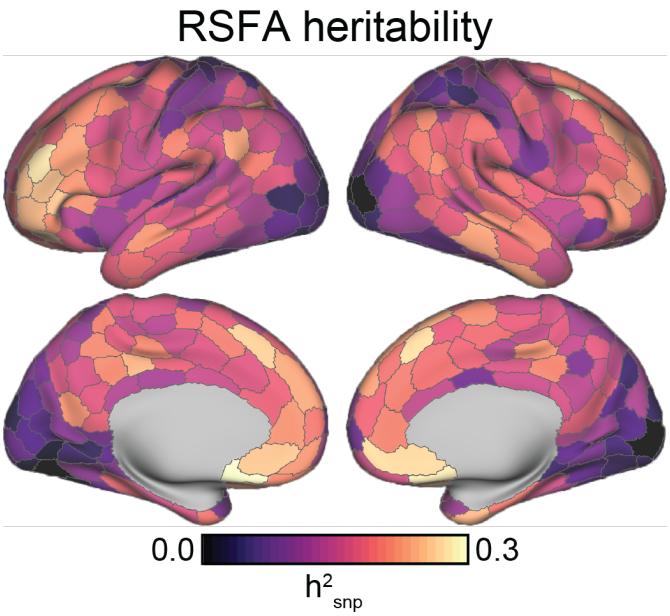

Supplemental Figure 5. SNP-wise heritability for each of the 400 bi-hemispheric cortical parcels from Schaefer and colleagues[47].

References

1. Cajal, S. R. Y. *Recollections of my life*. Translated by Craigie E.H. (Garland Publishing, Inc, 1988).
2. Kepecs, A. & Fishell, G. Interneuron cell types are fit to function. *Nature* **505,** 318–326 (2014).
3. Markram, H. *et al.* Interneurons of the neocortical inhibitory system. *Nature Reviews Neuroscience* **5,** 793–807 (2004).
4. Biswal, B. B. *et al.* Toward discovery science of human brain function. *Proc Natl Acad Sci USA* **107,** 4734–4739 (2010).
5. Nakazawa, K. *et al.* GABAergic interneuron origin of schizophrenia pathophysiology. *Neuropharmacology* **62,** 1574–1583 (2012).
6. Gonzalez-Burgos, G., Cho, R. Y. & Lewis, D. A. Alterations in cortical network oscillations and parvalbumin neurons in schizophrenia. *Biological Psychiatry* **77,** 1031–1040 (2015).
7. Lin, L. C. & Sibille, E. Somatostatin, neuronal vulnerability and behavioral emotionality. *Molecular Psychiatry* **20,** 377–387 (2015).
8. Richiardi, J. *et al.* Correlated gene expression supports synchronous activity in brain networks. *Science* **348,** 1238–1241 (2015).
9. Anderson, K. M. *et al.* Gene expression links functional networks across cortex and striatum. *Nature Communications* **9,** 1-14 (2018)
10. Krienen, F. M., Yeo, B. T. T., Ge, T., Buckner, R. L. & Sherwood, C. C. Transcriptional profiles of supragranular-enriched genes associate with corticocortical network architecture in the human brain. *Proc Natl Acad Sci USA* **113,** E469–E478 (2016).
11. Hawrylycz, M. *et al.* Canonical genetic signatures of the adult human brain. *Nat Neurosci* **18,** 1832–1844 (2015).
12. Burt, J. B. *et al.* Hierarchy of transcriptomic specialization across human cortex captured by structural neuroimaging topography. *Nat Neurosci* **27,** 889–15 (2018).
13. Kim, Y. *et al.* Brain-wide maps reveal stereotyped cell-type- based cortical architecture and subcortical sexual dimorphism. *Cell* **171,** 456–460.e22 (2017).
14. Hendry, S. H. C., Schwark, H. D., Jones, E. G. & Yan, J. Numbers and proportions of GABA-immunoreactive neurons in different areas of monkey cerebral cortex. *The Journal of Neuroscience* **7,** 1503–1519 (1987).
15. Douglas, R. J. & Martin, K. A. C. Mapping the matrix: The ways of neocortex. *Neuron* **56,** 226–238 (2007).
16. Kawaguchi, Y. & Kubota, Y. GABAergic cell subtypes and their synaptic connections in rat frontal cortex. *Cerebral Cortex* **7,** 476–486 (1997).
17. Chaudhuri, R., Knoblauch, K., Gariel, M.-A., Kennedy, H. & Wang, X.-J. A large-scale circuit mechanism for hierarchical dynamical processing in the primate cortex. *Neuron* **88,** 419–431 (2015).
18. Lee, J. H. *et al.* Global and local fMRI signals driven by neurons defined optogenetically by type and wiring. *Nature* **465,** 788–792 (2010).
19. Sohal, V. S., Zhang, F., Yizhar, O. & Deisseroth, K. Parvalbumin neurons and gamma rhythms enhance cortical circuit performance. *Nature* **459,** 698–702 (2009).
20. Cardin, J. A. *et al.* Driving fast-spiking cells induces gamma rhythm and controls sensory responses. *Nature* **459,** 663–667 (2009).
21. Nir, Y. *et al.* Coupling between neuronal firing rate, gamma LFP, and BOLD fMRI is related to interneuronal correlations. *Current Biology* **17,** 1275–1285 (2007).
22. Niessing, J. *et al.* Hemodynamic Signals Correlate Tightly with Synchronized Gamma Oscillations. *Science* **309,** 958–951 (2005).
23. Shmuel, A. & Leopold, D. A. Neuronal correlates of spontaneous fluctuations in fMRI signals in monkey visual cortex: Implications for functional connectivity at rest. *Hum. Brain Mapp.* **29,** 751–761 (2008).
24. Schölvinck, M. L., Maier, A., Ye, F. Q., Duyn, J. H. & Leopold, D. A. Neural basis of global resting-state fMRI activity. *Proc Natl Acad Sci USA* **107,** 10238–10243 (2010).
25. Magri, C., Schridde, U., Murayama, Y., Panzeri, S. & Logothetis, N. K. The amplitude and timing of the BOLD signal reflects the relationship between local field potential power at different frequencies. *The Journal of Neuroscience* **32,** 1395–1407 (2012).

26. Lewis, D. A., Curley, A. A., Glausier, J. R. & Volk, D. W. Cortical parvalbumin interneurons and cognitive dysfunction in schizophrenia. *Trends in Neurosciences* **35,** 57–67 (2012).
27. Miller, K. L. *et al.* Multimodal population brain imaging in the UK Biobank prospective epidemiological study. *Nat Neurosci* **19,** 1523–1536 (2016).
28. Mi, D. *et al.* Early emergence of cortical interneuron diversity in the mouse embryo. *Science* **360,** 81–85 (2018).
29. Wamsley, B. & Fishell, G. Genetic and activity-dependent mechanisms underlying interneuron diversity. *Nature Reviews Neuroscience* **18,** 299–309 (2017).
30. Wonders, C. P. & Anderson, S. A. The origin and specification of cortical interneurons. *Nature Reviews Neuroscience* **7,** 687–696 (2006).
31. Fogarty, M. *et al.* Spatial genetic patterning of the embryonic neuroepithelium generates GABAergic interneuron diversity in the adult cortex. *Journal of Neuroscience* **27,** 10935–10946 (2007).
32. Wonders, C. P. *et al.* A spatial bias for the origins of interneuron subgroups within the medial ganglionic eminence. *Developmental Biology* **314,** 127–136 (2008).
33. Hawrylycz, M. J. *et al.* An anatomically comprehensive atlas of the adult human brain transcriptome. *Nature* **489,** 391–399 (2012).
34. Bakken, T. E. *et al.* A comprehensive transcriptional map of primate brain development. *Nature* **535,** 367–375 (2016).
35. Sidman, R. L. & Rakic, P. Neuronal migration, with special reference to the developing human brain: A Review. *Brain Research* **62,** 1–35 (1973).
36. Letinic, K., Zoncu, R. & Rakic, P. Origin of GABAergic neurons in the human neocortex. *Nature* **417,** 645–649 (2002).
37. Fulcher, B. D. & Fornito, A. A transcriptional signature of hub connectivity in the mouse connectome. *Proc Natl Acad Sci USA* **113,** 1435–1440 (2016).
38. Buckner, R. L., Krienen, F. M. & Yeo, B. T. T. Opportunities and limitations of intrinsic functional connectivity MRI. *Nat Neurosci* **16,** 832–837 (2013).
39. Choi, E. Y., Yeo, B. T. T. & Buckner, R. L. The organization of the human striatum estimated by intrinsic functional connectivity. *Journal of Neurophysiology* **108,** 2242–2263 (2012).
40. Alexander, G. E., DeLong, M. R. & Strick, P. L. Parallel organization of functionally segregated circuits linking basal ganglia and cortex. *Annual Review of Neuroscience* 357–381 (1986).
41. Hwang, K., Bertolero, M. A., Liu, W. B. & D'Esposito, M. The human thalamus Is an integrative hub for functional brain networks. *Journal of Neuroscience* **37,** 5594–5607 (2017).
42. Haber, S. N. & Knutson, B. The reward circuit: Linking primate anatomy and human Imaging. *Neuropsychopharmacology* **35,** 4–26 (2009).
43. Menke, R. A., Jbabdi, S., Miller, K. L., Matthews, P. M. & Zarei, M. Connectivity-based segmentation of the substantia nigra in human and its implications in Parkinson's disease. *NeuroImage* **52,** 1175–1180 (2010).
44. Haber, S. N. The primate basal ganglia: parallel and integrative networks. *Journal of Chemical Neuroanatomy* **26,** 317–330 (2003).
45. Murray, J. D. *et al.* A hierarchy of intrinsic timescales across primate cortex. *Nat Neurosci* **17,** 1661–1663 (2014).
46. Kannurpatti, S. S. & Biswal, B. B. Detection and scaling of task-induced fMRI-BOLD response using resting state fluctuations. *NeuroImage* **40,** 1567–1574 (2008).
47. Schaefer, A. *et al.* Local-global parcellation of the human cerebral cortex from intrinsic functional connectivity MRI. *Cerebral Cortex* **28,** 3095–3114 (2018).
48. Bijsterbosch, J. *et al.* Investigations into within- and between-subject resting-state amplitude variations. *NeuroImage* **159,** 57–69 (2017).
49. Yang, J., Lee, S. H., Goddard, M. E. & Visscher, P. M. GCTA: A tool for genome-wide complex trait analysis. *The American Journal of Human Genetics* **88,** 76–82 (2011).
50. Wang, G.-Z. *et al.* Correspondence between resting-state activity and brain gene expression. *Neuron* **88,** 659–666 (2015).
51. Visscher, P. M. *et al.* 10 years of GWAS discovery: biology, function, and translation. *The American Journal of Human Genetics* **101,** 5–22 (2017).
52. Stein, J. L. *et al.* Identification of common variants associated with human hippocampal and intracranial volumes. *Nat Genet* **44,** 552–561 (2012).

53. Skene, N. G. *et al.* Genetic identification of brain cell types underlying schizophrenia. *Nat Genet* **50,** 825–833 (2018).
54. Fromer, M. *et al.* Gene expression elucidates functional impact of polygenic risk for schizophrenia. *Nat Neurosci* **19,** 1442–1453 (2016).
55. Lonsdale, J. *et al.* The Genotype-Tissue Expression (GTEx) project. *Nat Genet* **45,** 580–585 (2013).
56. Baker, J. T. *et al.* Disruption of cortical association networks in schizophrenia and psychotic bipolar disorder. *JAMA Psychiatry* **71,** 109–10 (2014).
57. Dienel, S. J. & Lewis, D. A. Alterations in cortical interneurons and cognitive function in schizophrenia. *Neurobiology of Disease* 1–11 (2018). doi:10.1016/j.nbd.2018.06.020
58. Schizophrenia Working Group of the Psychiatric Genomics Consortium. Biological insights from 108 schizophrenia-associated genetic loci. *Nature* **511,** 421–427 (2014).
59. de Leeuw, C. A., Mooij, J. M., Heskes, T. & Posthuma, D. MAGMA: generalized gene-set analysis of GWAS data. *PLoS Comput Biol* **11,** e1004219–19 (2015).
60. Euesden, J., Lewis, C. M. & O'Reilly, P. F. PRSice: Polygenic risk score software. *Bioinformatics* **31,** 1466–1468 (2015).
61. Felleman, D. J. & Van Essen, D. C. Distributed Hierarchical Processing in the Primate Cerebral Cortex. *Cerebral Cortex* **1,** 1–47 (1991).
62. Muthukumaraswamy, S. D., Edden, R. A. E., Jones, D. K., Swettenham, J. B. & Singh, K. D. Resting GABA concentration predicts peak gamma frequency and fMRI amplitude in response to visual stimulation in humans. *Proc Natl Acad Sci USA* **106,** 8356–8361 (2009).
63. Sullivan, P. F., Kendler, K. S. & Neale, M. C. Schizophrenia as a complex trait: Evidence from a meta-analysis of twin studies. *Arch Gen Psychiatry* **60,** 1187–1192 (2003).
64. Uhlhaas, P. J. & Singer, W. Abnormal neural oscillations and synchrony in schizophrenia. *Nature Reviews Neuroscience* **11,** 100–113 (2010).
65. Akbarian, S. *et al.* Gene expression for glutamic acid decarboxylase is reduced without loss of neurons in prefrontal cortex of schizophrenics. *Arch Gen Psychiatry* **52,** 258–266 (1995).
66. Mauney, S. A. *et al.* Developmental pattern of perineuronal nets in the human prefrontal cortex and their deficit in schizophrenia. *Biological Psychiatry* **74,** 427–435 (2013).
67. Enwright, J. F. *et al.* Transcriptome alterations of prefrontal cortical parvalbumin neurons in schizophrenia. *Molecular Psychiatry* 1–8 (2017). doi:10.1038/mp.2017.216
68. Yanagi, M. *et al.* Kv3.1-containing K+ channels are reduced in untreated schizophrenia and normalized with antipsychotic drugs. **19,** 573–579 (2013).
69. Marín, O. Interneuron dysfunction in psychiatric disorders. *Nature Reviews Neuroscience* **13,** 107–120 (2012).
70. Toker, L., Mancarci, B. O., Tripathy, S. & Pavlidis, P. Transcriptomic evidence for alterations in astrocytes and parvalbumin interneurons in subjects with bipolar disorder and schizophrenia. *Biological Psychiatry* 1–10 (2018). doi:10.1016/j.biopsych.2018.07.010
71. Fee, C., Banasr, M. & Sibille, E. Somatostatin-positive Gamma-Aminobutyric Acid interneuron deficits in depression: Cortical microcircuit and therapeutic perspectives. *Biological Psychiatry* **82,** 549–559 (2017).
72. Fuchs, T. *et al.* Disinhibition of somatostatin-positive GABAergic interneurons results in an anxiolytic and antidepressant-like brain state. *Molecular Psychiatry* **22,** 920–930 (2016).
73. Schmaal, L. *et al.* Cortical abnormalities in adults and adolescents with major depression based on brain scans from 20 cohorts worldwide in the ENIGMA Major Depressive Disorder Working Group. *Molecular Psychiatry* **22,** 900–909 (2016).
74. Ducharme, S. *et al.* Anxious/depressed symptoms are linked to right ventromedial prefrontal cortical thickness maturation in healthy children and young adults. *Cerebral Cortex* **24,** 2941–2950 (2014).
75. Holmes, A. J. *et al.* Individual differences in amygdala-medial prefrontal anatomy link negative affect, impaired social functioning, and polygenic depression risk. *Journal of Neuroscience* **32,** 18087–18100 (2012).
76. Wolfe, C. J., Kohane, I. S. & Butte, A. J. Systematic survey reveals general applicability of 'guilt-by-association' within gene coexpression networks. *BMC Bioinformatics* **6,** 227–10 (2005).
77. Elliott, M. L. *et al.* A polygenic score for higher educational attainment is associated with larger brains. *Cerebral Cortex* **491,** 56–9 (2018).

78. Duncan, L. *et al.* Analysis of polygenic score usage and performance across diverse human populations. *bioRxiv* 1–21 (2018). doi:10.1101/398396
79. Ge, T., Holmes, A. J., Buckner, R. L., Smoller, J. W. & Sabuncu, M. R. Heritability analysis with repeat measurements and its application to resting-state functional connectivity. *Proc Natl Acad Sci USA* **114,** 5521–5526 (2017).
80. Colclough, G. L. *et al.* The heritability of multi-modal connectivity in human brain activity. *eLife* **e20178,** 1–27 (2017).
81. Romme, I. A. C., de Reus, M. A., Ophoff, R. A., Kahn, R. S. & van den Heuvel, M. P. Connectome disconnectivity and cortical gene expression in patients with schizophrenia. *Biological Psychiatry* **81,** 495–502 (2017).
82. Kvitsiani, D. *et al.* Distinct behavioural and network correlates of two interneuron types in prefrontal cortex. *Nature* **498,** 363–366 (2013).
83. Johnson, W. E., Li, C. & Rabinovic, A. Adjusting batch effects in microarray expression data using empirical Bayes methods. *Biostatistics* **8,** 118–127 (2006).
84. Romero-Garcia, R. *et al.* Structural covariance networks are coupled to expression of genes enriched in supragranular layers of the human cortex. *NeuroImage* **171,** 256–267 (2018).
85. Marcus, D. S. *et al.* Informatics and data mining tools and strategies for the Human Connectome Project. *Frontiers in Neuroinformatics* **5,** 1–12 (2011).
86. Jenkinson, M., Bannister, P., Brady, M. & Smith, S. Improved optimization for the robust and accurate linear registration and motion correction of brain images. *NeuroImage* **17,** 825–841 (2002).
87. Beckmann, C. F. & Smith, S. M. Probabilistic independent component analysis for functional magnetic resonance imaging. *IEEE Trans. Med. Imaging* **23,** 137–152 (2004).
88. Cox, R. W. AFNI: Software for analysis and visualization of functional magnetic resonance neuroimages. *Computers and Biomedical Research* **29,** 162–173 (1996).
89. Purcell, S. *et al.* PLINK: A tool set for whole-genome association and population-based linkage analyses. *The American Journal of Human Genetics* **81,** 559–575 (2007).
90. Durinck, S. *et al.* BioMart and Bioconductor: a powerful link between biological databases and microarray data analysis. *Bioinformatics* **21,** 3439–3440 (2005).